Supplementary information for:

Membrane-Protein Binding Measured with Solution-Phase Plasmonic Nanocube Sensors

Contents

Supplementary Figure 1

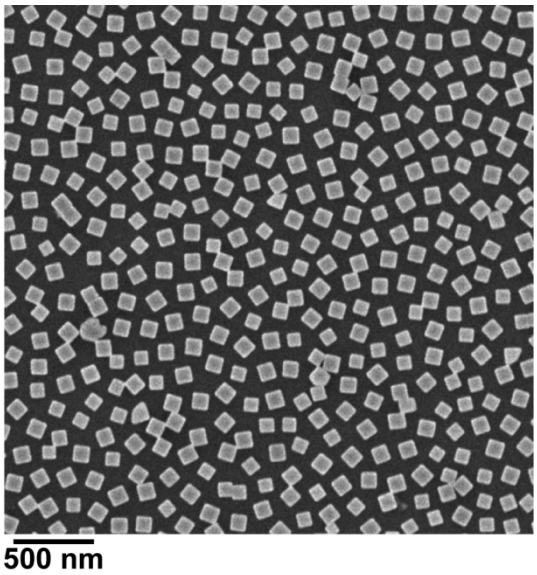

Figure S1. Scanning electron microscope (SEM) image of silver nanocube. Highly monodisperse nanocubes were synthesized using the polyol method.

Supplementary Figure 2

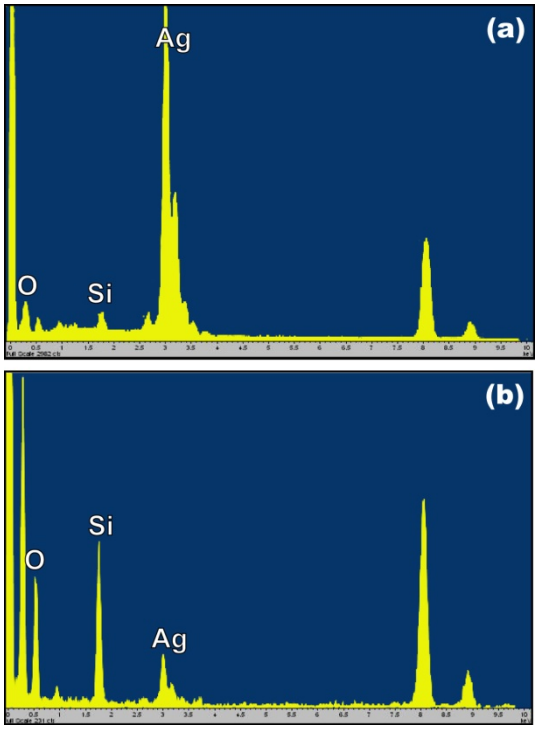

Figure S2. Energy-dispersive X-ray spectroscopy (EDS) spectra of $Ag@SiO_2$ nanocube. (a) EDS spectrum on the center of $Ag@SiO_2$ nanocube. (b) EDS spectrum on the silica shell of $Ag@SiO_2$ nanocube

Supplementary Figure 3

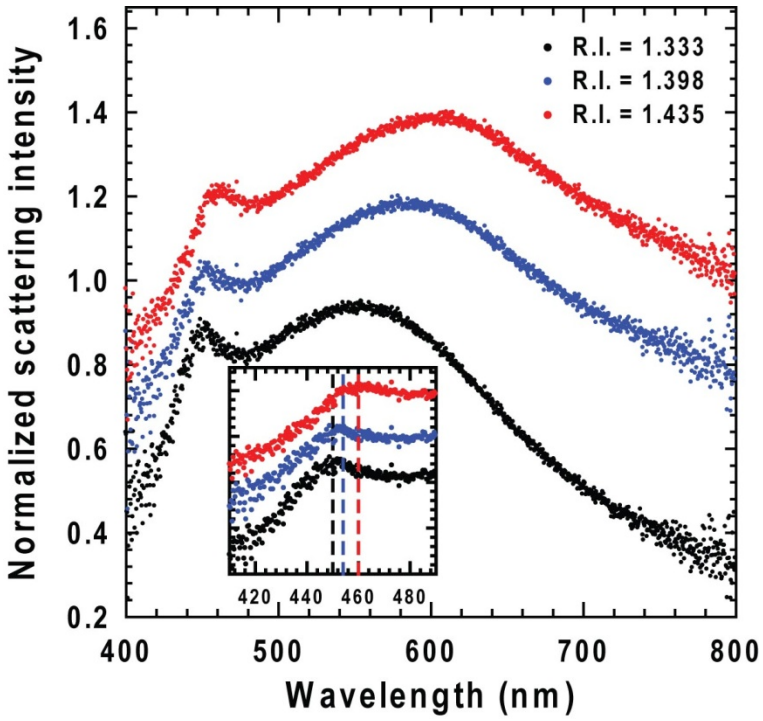

Figure S3. Dark field light scattering of nanocube in different refractive index (R.I.) media (water / glycerol solution). The spectra were detected with an inverted microscope coupled to a spectrometer. The inset shows the resolved details of quadrupolar peak. The dashed lines represent the position of maximum peak.

Supplementary Figure 4

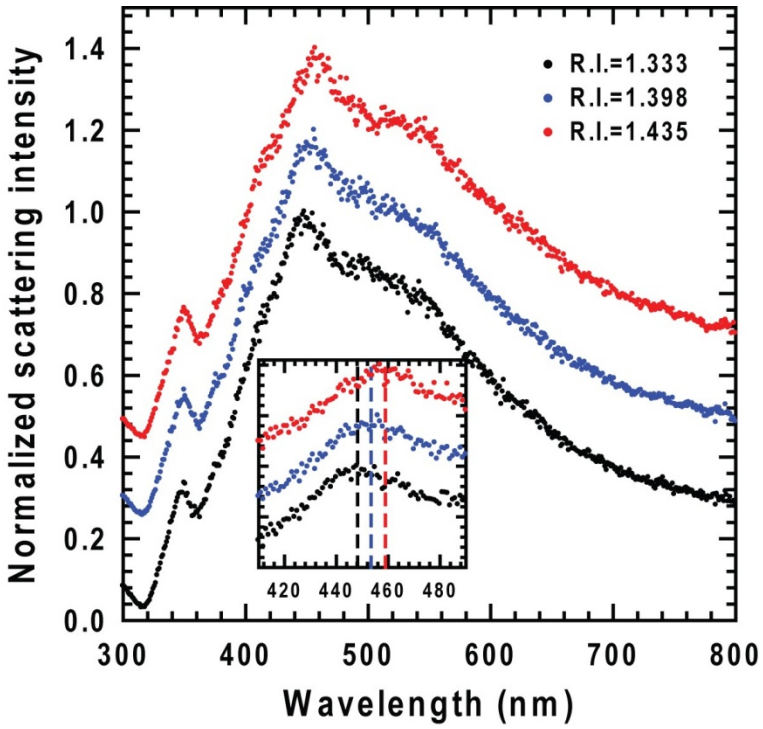

Figure S4. The light scattering spectra detected at a fixed angle (90 degree) in different refractive index (R.I.) media (water/glycerol solution) in a standard fluorescence spectrophotometer. The inset shows the resolved details of the quadrupolar peak. The dashed lines represent the position of the maximum peak.

Supplementary Figure 5

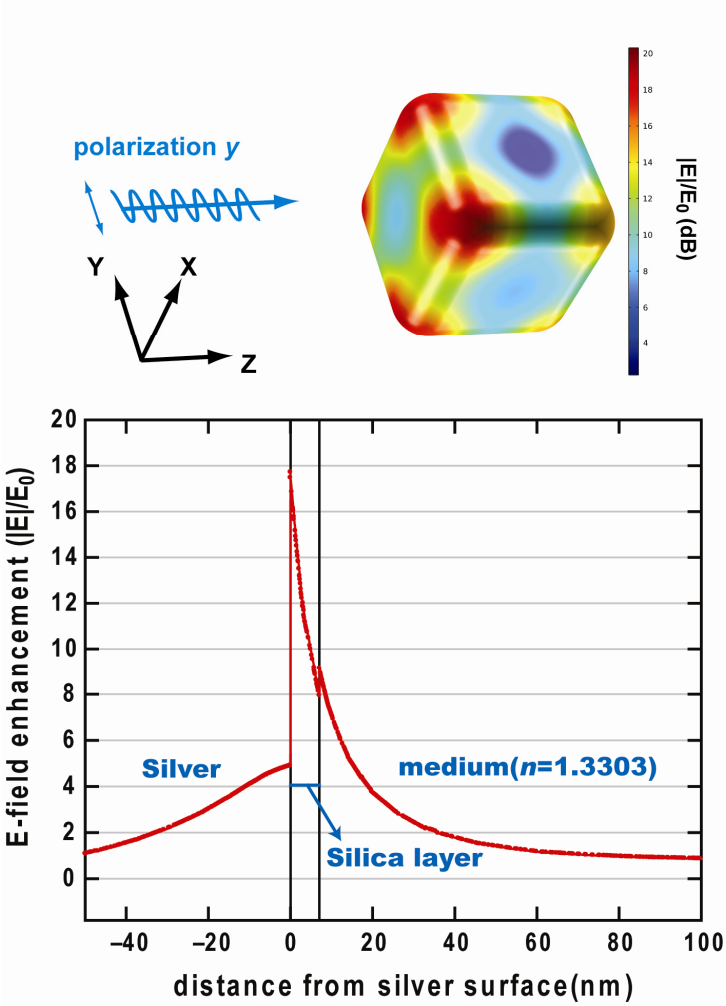

Figure S5. Electromagnetic field enhancement profile along the nanocube diagonal computed in FEA. The cross-section originates from the nanocube's center through a corner along the vector $(x,y,z) = (1,1,-1)$ in Fig. 1h. The model geometry of the silver nanocube was calculated from TEM, revealing a nanocube lateral dimension of 98 nm, 19 nm radius of curvature at the edges. The geometry of the silica shell was directly scaled up from silver nanocube to reach 4.0 nm shell thickness on facet, and thus the shell thickness through the corner is 7.0 nm in this cross-section.

Supplementary Figure 6

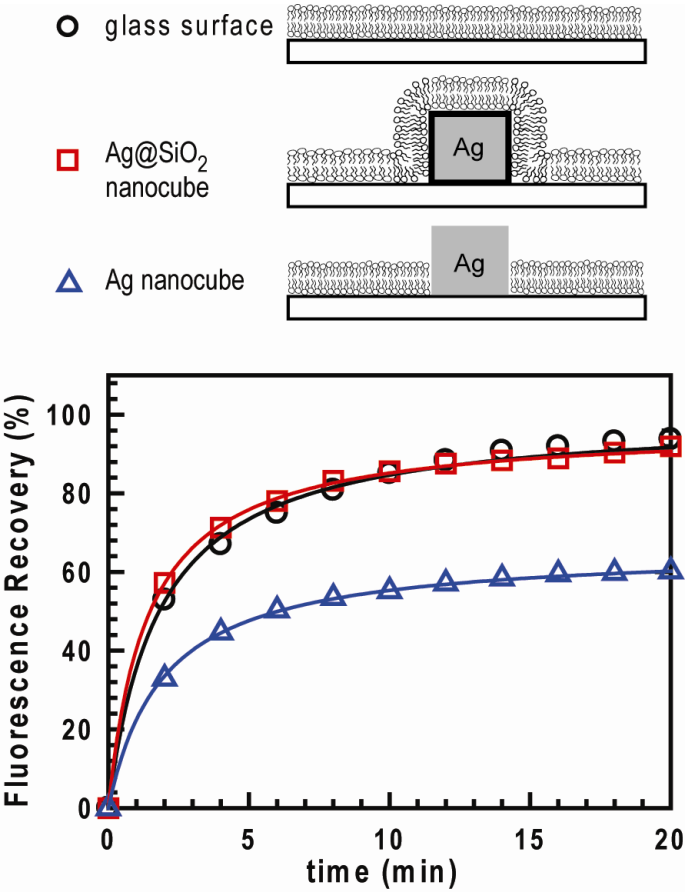

Figure S6. Normalized fluorescence recovery of supported lipid bilayers over three different substrates: (1) a bare glass surface, (2) Ag@SiO_2 nanocube adhered on a glass surface, and (3) Ag nanocube adhered on a glass surface. Nanocube-adhered substrates were prepared by drying a solution of nanocubes onto glass ($2 \cdot 10^8$ nanocubes on 18mm circle microscope cover glass). The two surfaces are expected to have similar nanocube densities after immobilization. No difference in recovery was observed between glass and Ag@SiO_2 nanocube substrates, although a higher immobile fraction was observed on the Ag nanocube substrate. Illustrations are not drawn to scale.

Supplementary Figure 7

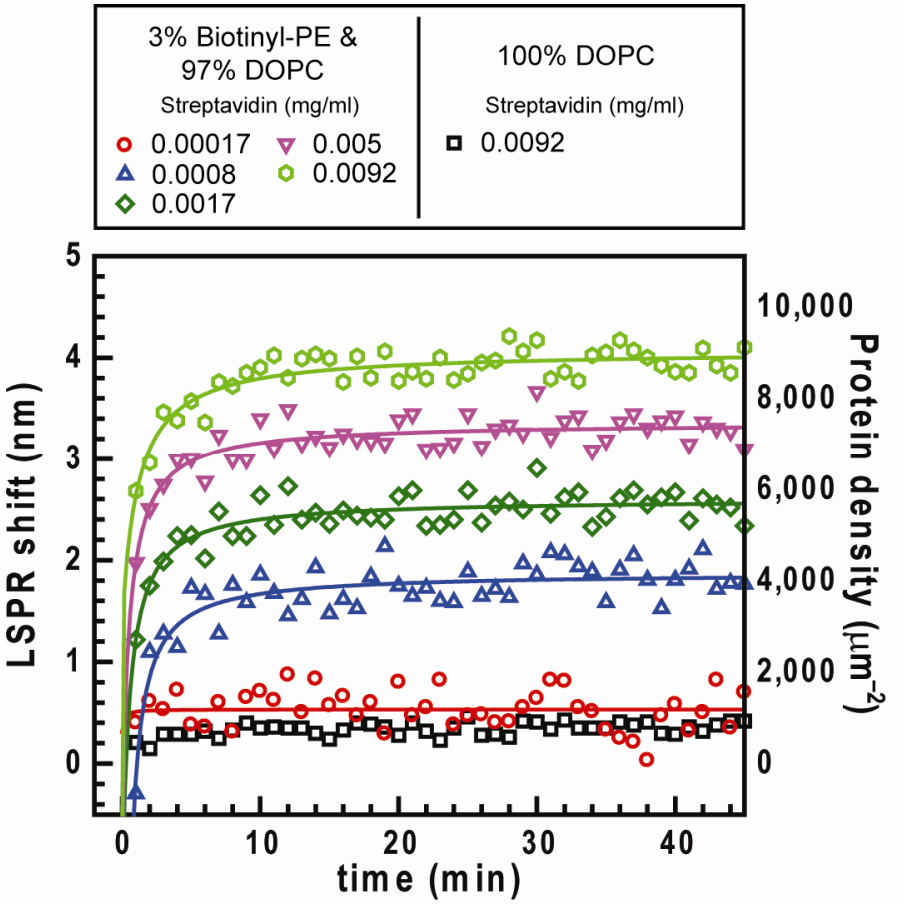

Figure S7. The kinetics of streptavidin binding to biotinylated lipid at different concentrations monitored by nanocube sensors. The biotinylated bilayer contains 3% biotinyl-cap-PE and 97% DOPC. The control bilayer is 100% DOPC. Fifteen consecutive LSPR spectra were collected to obtain an average baseline prior to kinetics measurements. Higher concentrations of streptavidin result in stronger shifts in the LSPR spectra. Streptavidin does not bind in the negative control bilayer (100% DOPC) and expectedly shows no LSPR shift.

Supplementary Figure 8

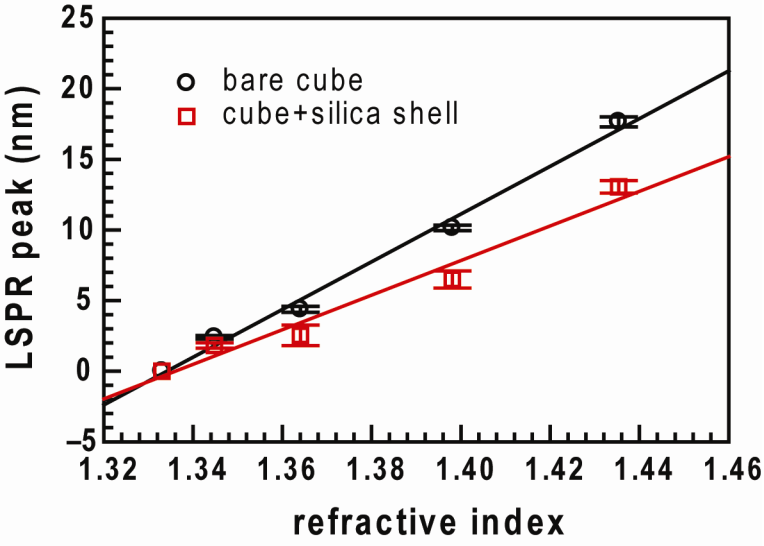

Figure S8. The LSPR shift of Ag and Ag@SiO_2 nanocubes in various refractive index media (water / glycerol solution). The averages and standard deviations of 3 different synthesis batches are presented. Ag@SiO_2 nanocubes show less sensitivity to refractive index change of media. The Ag nanocubes had a shift of 169 nm / RIU whereas the Ag@SiO_2 nanocubes had a shift of 123 nm / RIU.

Supplementary Figure 9

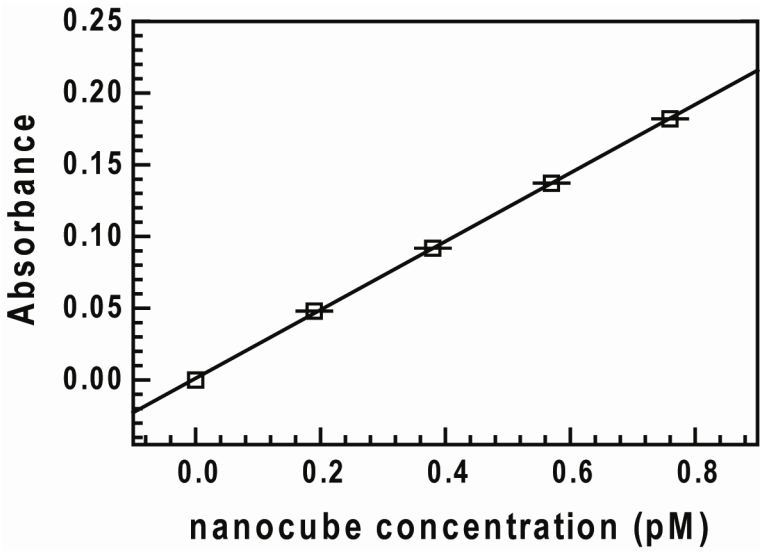

Figure S9. The correlation between maximum absorbance of quadrupolar peaks and nanocube concentration. Nanocubes deposited onto sedimentation chambers were directly imaged by dark field scattering microscopy. The linear relation between particle concentration and absorbance provides an approach to easily determine the nanocube concentration during the binding measurement[1]. (n=20, mean ± s.d.)

Supplementary Figure 10

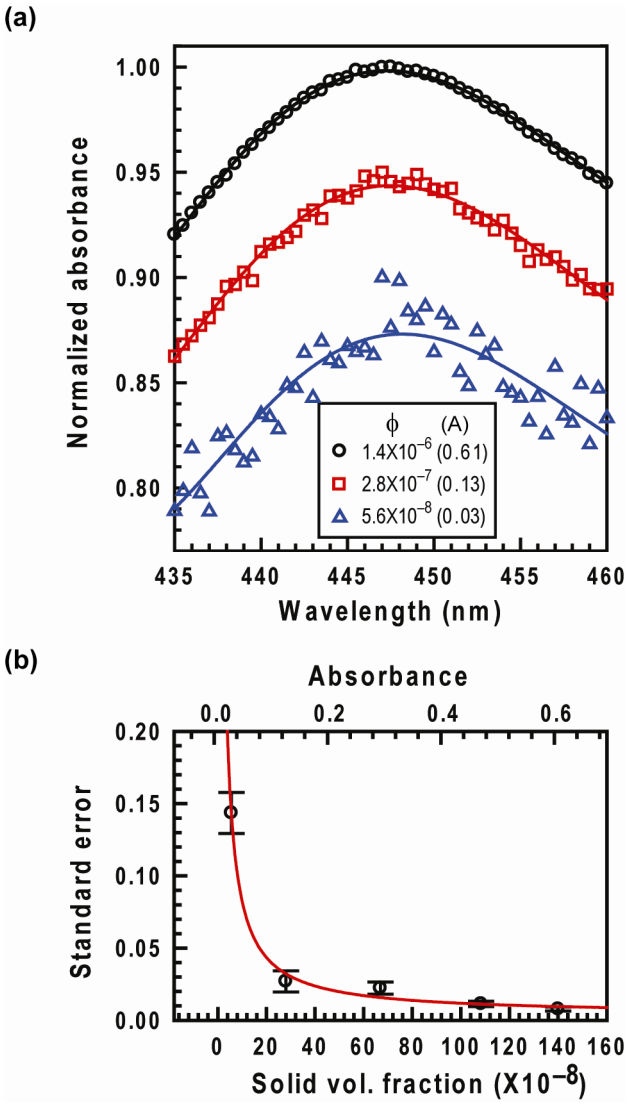

Figure S10. Estimated error of LSPR measurement. (a) LSPR spectra with various nanocube concentrations. The symbols and solid lines represent the raw data and the polynomial fits at different nanocube concentrations (solid volume fraction ϕ and maximum absorbance A). Lower concentrations of nanocubes show a lower signal-to-noise ratio and result in larger deviations of polynomial fits. (b) The standard error of 20 continuous measurements at different nanocube concentrations. (n=3, mean ± s.d.)

Supplementary Figure 11

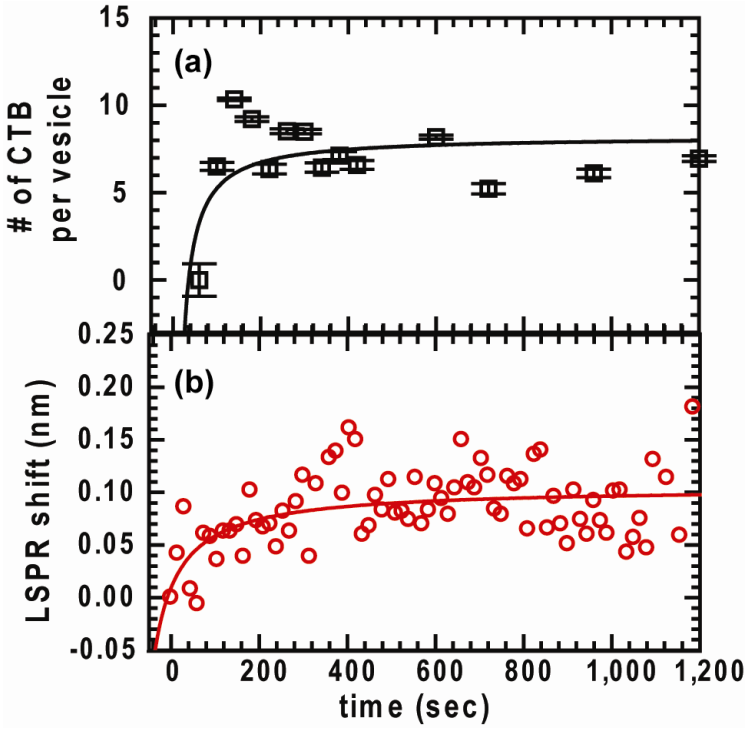

Figure S11. CTB binding measurements using FCS and nanocube assay. (a) The kinetics of Alexa 594-CTB binding to vesicles containing G_{M1} lipid monitored by multi-component FCS. (n=20, mean ± s.d.) (b) The kinetics of Alexa 594-CTB binding to supported lipid bilayer on Ag@SiO_2 nanocubes.

Supplementary Table 1

The summary of protein surface density per LSPR peak shift. The protein densities per LSPR shift measured by streptavidin titration, biotinyl-cap-PE titration, and fluorescence assay were evaluated from the slopes in Fig.2a. The value measured by FCS is calculated from the average LSPR shift after 1000 sec in Fig.2b. The average response determined by biotin-streptavidin system was 0.191 ng mm^{-2} nm^{-1}, consistent with the FCS measurements. Error limits are derived from the statistical error of curve fitting.

	# of protein / nanocube /LSPR shift (nm^{-1})	protein number density/ LSPR shift (μm^{-2} nm^{-1})	protein mass density/ LSPR shift (ng mm^{-2} nm^{-1})
Streptavidin-biotin system			
Streptavidin titration	138±12	2033±180	0.178±0.016
biotin titration	135±37	1996±57	0.175±0.048
fluorescence assay	170±23	2512±352	0.220±0.031
		Average :	0.191±0.025
CTB-G_{M1} system			
FCS	141±16	2084±234	0.191±0.021

Supplementary Discussion

Calibration of nanocube concentration and error of LSPR measurement

Determination of nanocube concentration in solution is necessary to evaluate the membrane surface area for kinetics calculations. To address this, nanocubes deposited onto sedimentation chambers were directly imaged by dark field scattering microscopy. A homemade image analysis program was developed to count the number of nanocubes in each imaging area. In addition, the nanocube concentration can be simply determined by measuring the absorbance using a UV-vis spectrophotometer (Supplementary Fig.9). The linear relation between particle concentration and absorbance was then used to determine the nanocube concentration during the binding measurement[1].

The prominent quadrupolar LSPR peak λ_{max} was interpolated by a polynomial fit. The higher concentration sample predictably provided a higher signal-to-noise ratio and hence higher precision of λ_{max} (Supplementary Fig.10a). The relation between precision of λ_{max} and nanocube concentration is shown in Supplementary Fig.10b. To obtain 0.01 nm precision of $\lambda_{max,}$ working concentration of nanocube measurement is at absorbance larger than 0.4. For 10 mm optical pathlength of spectrometer cells, 0.4 absorbance corresponds to the solid volume fraction 10^{-6} (Supplementary Fig.10b).

This solution-based sensing platform allows the analysis of ensembles in excess of 10^{12} nanocubes. In contrast to conventional LSPR assays, taking large ensemble measurements in solution reduces inaccuracies in the LSPR response caused by particle and bilayer variations thus increasing sensitivity and overall confidence in the measurement. Our calibration results provide the optimal working concentrations for the nanocube measurements. The high absorption of the nanocube sample, along with the narrow LSPR peak, results in highly precise interpolation of tiny shifts in λ_{max}. For the $Ag@SiO_2$ nanocube covered with 100% DOPC bilayer, the best resolution of LSPR measurements with a current UV-vis spectrophotometer is 0.01nm standard error of 20 consecutive scans (standard deviation=0.04 nm). It is correspondent to a protein density change of $\sim 1.9 \cdot 10^{-9}$ ng / μm^2. This indicates that the ideal sensitivity of the nanocube measurement can reach ~22 proteins /. μm^2 or 1.2 proteins per nanocube for a 53k Da size protein. The influences of protein binding may further introduce intrinsic fluctuation of signal. For example, the standard deviation of 20 measurements in Ste5 mutant system is 0.04 nm and standard error is 0.0l nm that is closed to ideal sensitivity. For Ste5 wildtype, the standard deviation and error is 0.065 nm and 0.015 nm that is a little bit higher. (Fig.2c)

Calibration of LSPR shifts vs. protein density

To further calibrate the correlation between LSPR shift and protein surface density on the membrane, three different approaches, (1) titrating biotinyl-cap-PE in bilayer, (2) titrating streptavidins in solution, and (3) measuring unbound fluorescent streptavidins, were employed here. The first approach is to alter the mole fractions of biotinyl-cap-PE in bilayer (0%, 0.025%, 0.05%, 0.1%, and 0.2 %). The bilayer coated $Ag@SiO_2$ nanocubes were incubated with excess streptavidin. By assuming a DOPC lipid footprint in supported bilayers of 0.72 nm^2, the average surface density of streptavidin was be calculated[2]. This approach varies the number of biotin binding sites on the membrane surface to calibrate the dependence of the LSPR shift on protein surface density.

The second approach is to change the protein density on the membrane surface by titrating the streptavidin concentration. A fixed number of small unilamellar vesicles (SUVs, 97% DOPC + 3% biotinyl-cap-PE) mixed with $Ag@SiO_2$ nanocubes were incubated with different amount of streptavidin. Because of the high affinity of biotin-streptavidin binding, we assume all streptavidin binds evenly and completely to vesicles and bilayers on $Ag@SiO_2$ nanocubes. The average streptavidin surface density on nanocubes can be evaluated by using a DOPC lipid footprint in supported bilayers.

In these two methods, we assume binding processes were complete after three hours incubation. Although previous a study shows the diffusion limitations of streptavidin binding to immobilized biotin are negligible[3], limited protein diffusion might erroneously lead to different calculated protein densities. Therefore, we introduce a third approach that measured unbound protein in the solution using streptavidin labeled with Alexa Fluo 647. In this approach, bilayer-coated $Ag@SiO_2$ nanocubes were incubated with different amount of fluorescent streptavidin for one hour. To separate bound from unbound streptavidin, streptavidin attached to bilayer-coated $Ag@SiO_2$ nanocubes was pulled down in a centrifuge. The concentration of unbound streptavidin remaining in the supernatant was determined by its fluorescence intensity in a spectrometer. Because nanocube concentration is known, the average streptavidin density on nanocubes was evaluated. To reduce the experimental error of fluorescent measurements, this approach required high nanocube concentrations to modulate the fluorescence intensity in supernatant.

Direct comparison of multi-component fluorescent correlation spectroscopy and nanocube detection

Fluorescence Correlation Spectroscopy (FCS) is a quantitative tool to locally measure molecular mobility and number densities of fluorescently labeled species[4]. In multi-components FCS measurements, we first determined the average number of vesicles and

CTB concentrations separately. Then, the same amount of vesicle and CTB were mixed to observe the kinetics of CTB binding.

The average number of vesicles N_v diffusing within the excitation spot was measured by FCS of vesicles doped with 0.5% BODIPY-FL-DHPE. These were performed with 488nm laser excitation at 0.2 mg / ml vesicle concentration. Twenty 120 sec measurements were taken and averaged to obtain statistical variations and fitted to an analytical expression of normal 3-D diffusion in a 3D-Gaussian volume for single diffusion species:

$$G(\tau) = \frac{1}{N} \frac{1}{1+\frac{\tau}{\tau_D}} \frac{1}{\sqrt{1+s^2 \frac{\tau}{\tau_D}}} \qquad \text{Eq (1)}$$

where N is the total number of diffusing particles, τ_D is the characteristic diffusion time, and s is a structure factor calibrated by a fluorescein standard. The average number of vesicles diffusing within the excitation spot N_v is equal to *1/G(0)* from the analytical fitting result. With the same approach, the number of Alexa 594-CTB diffusing within the excitation spot, N_{CTB}, was measured under 568nm laser excitation. The concentration of Alex 594-CTB was 0.004 mg / ml. Finally, the same amount of Alexa 594-CTB (0.004 mg / ml) was mixed with vesicle solution (0.2mg / ml) to reach the same concentration as the previous separate measurements. Then, the time-resolved concentration was obtained by performing a 30 sec measurement every minute using 568 nm laser excitation. For each FCS curve, the value of *G(0)* was extrapolated by fitting the curve to Eq. 1. Although Eq. 1 cannot fully describe multiple diffusing components with different brightnesses, it is sufficient to determine the value of *G(0)*.

The general expression for multicomponent 3-D diffusion is:

$$G(\tau) = \frac{1}{(\sum Q_k N_k)^2} \sum Q_j^2 N_j \frac{1}{1+\frac{\tau}{\tau_{Dj}}} \frac{1}{\sqrt{1+s^2 \frac{\tau}{\tau_{Dj}}}} \qquad \text{Eq(2)}$$

where Q_k is the average brightness for the component k. In this study, we simplified the system into two components, freely diffusing and vesicle-bound Alexa 594-CTB. We assumed the average number of Alexa 594-CTB binding to one vesicle was σ. Thus, the average brightness of the CTB component on one vesicle is σ times brighter than freely diffusing Alexa 594-CTB. It has been shown that a single Q can be used to accurately represent the average properties of the true distribution in this type of measurement [4, 5].

The *G(0)* value of equation (2) can then be expressed as

$$G(0) = \frac{N_f + \sigma^2 N_v}{\left(N_f + \sigma N_v\right)^2} \qquad \text{eq(3)}$$

where σ is the number of bound CTB per vesicle, and N_f is the number of freely diffusing Alexa 594-CTB, which can be calculated from $N_f = N_{CTB} - \sigma N_V$. Using the measured N_v, N_{CTB}, and $G(0)$ values, the unknown σ can be computed from Eq (3). With the known average size of vesicles (120 nm), the surface density of CTB bound to vesicle can then be calculated (Supplementary Fig.11a).

For direct comparison, nanocube measurements were performed under the same experimental conditions as FCS. The same vesicle concentration used in FCS experiments was mixed with $Ag@SiO_2$ nanocubes to form supported lipid bilayers. Excess vesicles were not removed in order to maintain the same concentration of G_{M1} binding sites in the solution. The same amount of Alexa 594-CTB was added to the solution. Assuming that CTB binds equally to vesicles and bilayer-coated $Ag@SiO_2$ nanocubes, the surface density of bound CTB is the same on both surfaces. LSPR shifts were then monitored using a UV-Vis spectrophotometer (Supplementary Fig.11b). The LSPR shifts were converted to surface density using the LSPR response to protein mass change measured in the biotin-streptavidin system (0.191 ng mm^{-2} nm^{-1}, Supplementary Table 1). Kinetic binding curves measured by FCS and the nanocube assay reached equilibrium after 1000 sec (Supplementary Fig.11). The suitable working range for FCS depends on the size of the detection volume and the brightness of the fluorophores, and it typically falls below 100 nM [6]. Because concentration fluctuations from the ensemble average are crucial for FCS, these experiments were performed at a relatively low protein concentration and hence lower LSPR shift. Although the kinetic binding curves show a lower signal-to-noise ratio under such experimental conditions, the binding curves and final bound CBT density obtained from the two methods still show excellent agreement. In contrast to FCS, the detection of nanocube assay is not limited by analyte concentration because it measures the change of local refractive index. Practically, we have successfully performed protein binding measurement at concentration in the hundreds of micromolar range.

Detergent effect

During the measurement of Ste5-PH domain binding on supported phospholipid bilayers, we speculated that desorption of the lipid bilayer could influence the LSPR response. From our observations, adding detergent caused a blue shift that we attribute to disruptions of the bilayer. Detergents with low critical micelle concentration and high molecular weight are difficult to

remove by either dialysis or gel filtration[7]. Our results suggest that the use of detergent should be eliminated in all protein preparation steps for membrane protein binding measurements. In this paper, the use of detergent was therefore eliminated during protein purification to avoid these effects.

Reference

1. Haiss, W., Thanh, N.T.K., Aveyard, J. & Fernig, D.G. *Anal. Chem.* **79**, 4215-4221 (2007).

2. Vacklin, H.P., Tiberg, F. & Thomas, R.K. *Biochim. Biophys. Acta, Biomembr.* **1668**, 17-24 (2005).

3. Balgi, G., Leckband, D.E. & Nitsche, J.M. *Biophys. J.* **68**, 2251-2260 (1995).

4. Middleton, E.R. & Rhoades, E. *Biophys. J.* **99**, 2279-2288 (2010).

5. Pu, M.M., Fang, X.M., Redfield, A.G., Gershenson, A. & Roberts, M.F. *J. Biol. Chem.* **284**, 16099-16107 (2009).

6. Krichevsky, O. & Bonnet, G. *Rep. Prog. Phys.* **65**, 251-297 (2002).

7. Rigaud, J.L., Levy, D., Mosser, G. & Lambert, O. *Eur. Biophys. J.* **27**, 305-319 (1998).